Facile Fabrication of PbS Nanocrystal:C_{60} Fullerite Broadband Photodetectors with High Detectivity

*Rinku Saran, Muhammad N. Nordin, and Richard J. Curry**

Hybrid PbS nanocrystal/C_{60} fullerite photodetectors are fabricated using a simple one-step drop casting procedure onto pre-patterned interdigitated electrodes. The devices exhibit a broad spectral response from the near UV through to the near infrared yielding a detectivity, D^*, of above 10^{10} Jones from 400 nm to ≈1050 nm. The ability to further extend the spectral response to wavelengths ≈1350 nm in the near infrared via tuning of the PbS nanocrystal diameter is also demonstrated. The dynamic responses of the devices are presented, exhibiting a fast photocurrent rise time (<40 ns) followed by a long bi-exponential decay with characteristic lifetimes of τ_1 = 5.3 μs ± 0.1 μs and τ_2 = 37.8 μs ± 0.7 μs. These devices, which have a detectivity approaching that of commercial detectors, a broader spectral response, and a fast rise time, offer an attractive low-cost solution for large-area broadband photodetectors.

1. Introduction

Light detection in the ultraviolet (UV), visible and infrared (IR) regimes has a wide range of commercial and scientific applications that include imaging,[1] spectroscopy,[2] communication,[3] biomedical applications,[4,5] and night vision.[6] Today commercially available photodetectors are typically made from silicon carbide (SiC), silicon (Si) and indium gallium arsenide (InGaAs) for detection in UV, visible and near-IR regimes, respectively. It is highly desirable to have a single, low cost, multi-spectral range photodetector that covers the optical window created by present technologies and does not require cryogenic temperature for efficient operation. Organic materials are attractive as a low-cost solution, except for the fact that their spectral response is usually limited to the visible spectrum. There are few reports of organic photodetectors with broadband spectral response extending into the near-IR (i.e., beyond ≈700 nm). Those that exist are mainly based on small band gap conjugated polymers and still do not provide access to the majority of this spectral region.[7–10] Recently PbS nanocrystals (NCs) have emerged as an alternative promising candidate material for realizing broadband photodetectors. In particular, they offer solution processability and tunable absorption (via control of quantum confinement) displaying spectral sensitivity from the near-UV through to the near-IR.[11] Extensive research on PbS NC photodetectors has led to devices being reported yielding high detectivities (≈10^{12}–10^{13} Jones).[12–15]

One dimensional (1D) nanostructures of organic and inorganic materials have also gained interest for sensing and photodetector applications.[16–19] In particular, C_{60} has been widely studied due to its excellent electronic properties, which include n-type behavior,[20] a strong electron accepting nature, a high carrier mobility and superconductivity.[21] C_{60} nanostructures have potential application in transistors,[22] radio frequency (RF) detectors,[23] optical switches,[24] ring oscillators,[25] catalyst[26] and photovoltaics.[27,28] Various easy and rapid methods have been reported for the preparation of crystalline nanostructures of C_{60} (fullerites) including nanorods, nanowhiskers and nanosheets.[29–33] Reported 1D fullerites are highly crystalline in nature and have a high length to diameter ratio (1 mm:250 nm).[34] In addition, the most striking feature of C_{60} fullerites is their high electron mobility of ≈11 $cm^2 V^{-1} s^{-1}$, which is one of the highest reported values for an organic material.[35] For device applications, a method for uniform distribution of C_{60} nanorods has also been reported.[36] The individual relative merits of PbS NCs and C_{60} fullerites are therefore highly motivational for the development of hybrid organic-inorganic devices with the potential to provide a low-cost broadband detector technology.

C_{60} needle-like crystals photosensitized by semiconductor NCs was first reported by Biebersdorf et al.[37] Charge transfer from the NCs to C_{60} crystals, together with the high electron mobility in C_{60} crystals, resulted in significant improvement in the device photocurrent. Though controlled fabrication of such devices proved challenging, this work was followed by employing [6,6]-phenyl-C_{61}-butyric acid methyl ester (PCBM) in place of C_{60} crystals. The blend consisting of PCBM and PbS NCs capped with oleic acid ligands showed a detectivity of 2.5×10^{10} Jones at 1200 nm measured under high vacuum conditions (1×10^{-6} mbar).[38] A fast (f_{3dB} > 300 kHz) operating planar photodetector was also reported by introducing an interfacial recombination process that utilized a bilayer structure consisting of PbS NCs and PCBM.[39] Hybrid organic-inorganic photodetectors consisting of blends of PbS NCs, PCBM and poly(3-hexylthiophene) (P3HT) have also been reported.[1,40] For the further advancement of such devices charge transfer studies in blends incorporating PbS NCs, PCBM and P3HT were also carried out.[41,42] However, such devices require a

R. Saran, M. N. Nordin, Dr. R. J. Curry
Advanced Technology Institute
Department of Electronic Engineering
University of Surrey
Guildford, Surrey, GU2 7XH UK
E-mail: r.j.curry@surrey.ac.uk

DOI: 10.1002/adfm.201202818

multistep fabrication process which includes the deposition of electrodes to form a vertical sandwich type of device. This type of geometry then requires the use of transparent electrodes to allow light to enter the active region efficiently thus limiting their potential application and increasing cost.

For photodetector applications, charge transfer studies from PbS NCs to C_{60} fullerites have not been reported to date. C_{60} fullerites, due to their crystalline nature, offer a potentially higher mobility as compared to C_{60} films and PCBM and present modified optoelectronic properties. In addition, improved electron transfer is expected from PbS NCs to C_{60} fullerite crystals due to the lower lowest unoccupied molecular orbital (LUMO) of C_{60} (≈4.5 eV)[43,44] as compared to PCBM (≈3.7–4.2 eV).[7,45,46] Previously, no charge transfer was found from PbS NCs to PCBM for NCs above a diameter of ≈4.4 nm,[47,48] which restricts its application for photodetectors operating beyond ≈1300 nm. As per previously reported LUMO values of C_{60} and PbS NCs,[49] photoexcited electron transfer is favorable in such composites even for NC diameters above 6.6 nm extending its spectral response to 1600 nm and beyond.[27] Furthermore, the charge transfer process in such composites is still the focus of research, in particular with regard to the effect of NC ligand on the photodetector performance.

In this work, we demonstrate a hybrid C_{60} fullerite-PbS NC photodetector exhibiting a detectivity (D^*) ≈ 10^{10} Jones across the broad wavelength range from 400 nm to 1100 nm. The planar photodetector design employed also offers several advantages over conventional vertical sandwiched type structures including: i) ease of integration into read out circuits; ii) use of single metal electrodes; and iii) the removal of the need for a top electrode to improve light detection and avoid the requirement of a transparent conducting substrate.[50] Improved photoconductivity in the near-IR regime is achieved via sensitization of C_{60} fullerites by the PbS NCs. Charge transfer from PbS NCs to C_{60} fullerites is improved significantly following the exchange of long oleic acid NC ligands by short-chain carboxylic ligands. We evaluate the performance of the device by characterizing the device for planar photodetector application.

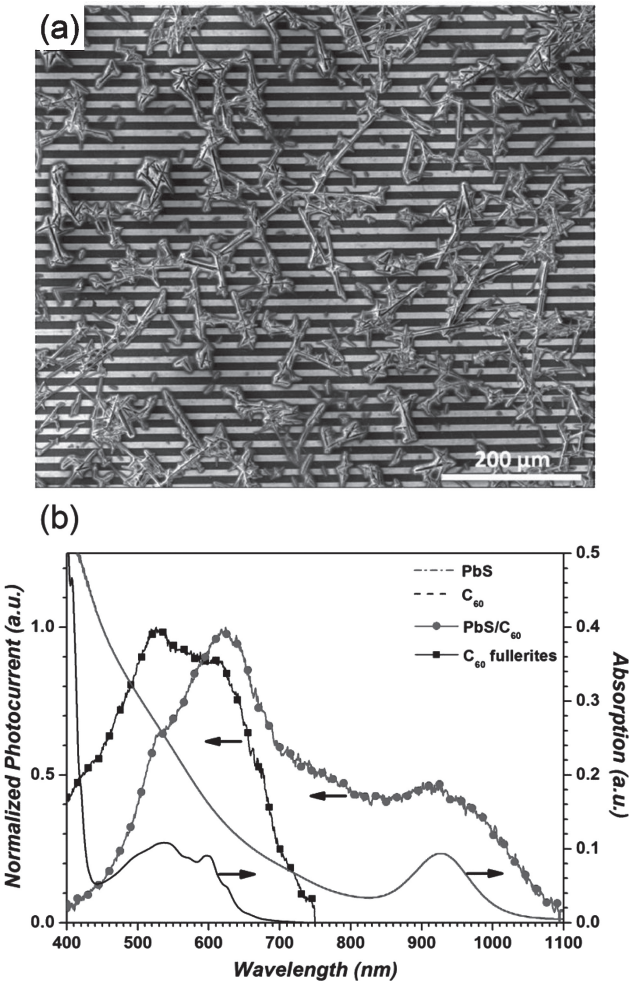

Figure 1. a) Scanning electron microscopy (SEM) image of a typical PbS NC/C_{60} fullerite device fabricated via drop casting C_{60} fullerites onto 10 µm wide interdigitated gold electrodes (electrode spacing = 10 µm). b) Normalized photocurrent spectra of a C_{60} fullerite only (squares) and PbS NC/C_{60} fullerite (circles) device. Also shown are the absorption spectra of C_{60} in m-xylene and PbS NCs in toluene.

2. Results and Discussion

C_{60} fullerites were prepared using the liquid-liquid interfacial precipitation (LLIP) method modified via the introduction of PbS NCs during the procedure. The resulting product was subsequently drop cast onto a set of 10 µm wide interdigitated gold (Au) electrodes with 10 µm spacing fabricated on a SiO_2 (250 nm) on Si substrate to form the device, **Figure 1**a. Using this simple method large area devices can be fabricated in a single step with those tested being 25 mm^2 (Supporting Information Figure S1a). The length of the C_{60} fullerites range from ≈1 to ≈125 µm with a skewed distribution peaking at ≈8 µm and a full width at half maximum of ≈10 µm (Supporting Information Figure S1b).

The photocurrent spectrum obtained from a typical C_{60} fullerite only and PbS NC/C_{60} fullerite device is shown in Figure 1b, normalized to their respective maxima, along with the absorption spectrum of C_{60} and PbS NCs. The wavelength dependent photocurrent obtained from the PbS NC/C_{60} fullerite device extends over both the visible and near-IR, significantly improving spectral coverage compared to that obtained via the use of C_{60} fullerites alone. The near-IR photocurrent also closely follows the measured absorption spectrum obtained from the PbS NCs strongly implying that they are the origin of this contribution. Devices fabricated via drop-casting PbS NCs alone did not yield any measurable photocurrent suggesting that the near-IR photocurrent occurs following a charge transfer process from the PbS NCs to the C_{60} fullerites. Close inspection of the PbS NC/C_{60} fullerite device photocurrent spectrum in the visible reveals peaks at ≈520 nm, ≈620 nm and ≈680 nm corresponding with C_{60} absorption features and those found within the C_{60} fullerite only device photocurrent spectrum. This implies that in the PbS NC/C_{60} fullerite devices, C_{60} fullerite dominates in contribution to the photocurrent in the visible range as compared to PbS NC, despite the fact that PbS NCs display strong optical absorption in the visible. Thus, we

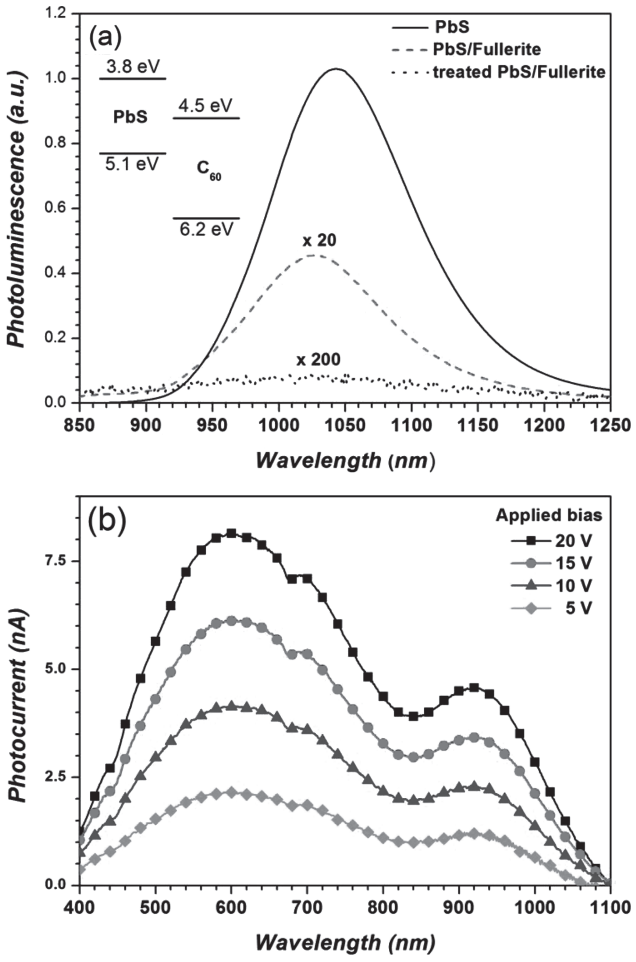

Figure 2. a) Photoluminescence spectra of PbS NC film (solid line) and a PbS NC/C_{60} fullerite composite film before (dashed line) and following (dotted line) ligand exchange. Inset to (a) shows a schematic energy level diagram of PbS NCs and C_{60}. b) Photocurrent spectra obtained from a PbS NC/C_{60} fullerite device following ligand exchange as a function of applied bias.

conclude that presence of PbS NCs not only increases the C_{60} fullerite photoconductivity but also extends its response to near-IR wavelengths (Supporting Information Figure S2a).

The relative energy level alignment between PbS NCs and C_{60} favors photoexcited electron transfer from PbS NCs to C_{60}. A schematic of energy level alignment of the PbS NCs used and C_{60} is shown inset to **Figure 2**a. Upon photoexcitation of the PbS NC/fullerite composite in the visible regime, excitons are generated in both the PbS NCs and C_{60}. It is then possible for electron transfer from a PbS NC to C_{60} to occur whilst the holes remain in PbS NC. However, due to the presence of the oleic acid capping ligands surrounding the PbS NCs the efficiency of this electron transfer process may be suppressed. Nonetheless, any transferred electrons not only have the potential to directly contribute to the photocurrent but may also be utilized in filling the C_{60} trap states,[37] thereby enhancing the photoconductivity of C_{60} fullerites. These electrons may then undergo back-transfer to the PbS NCs through an interfacial recombination process. Such a process can be efficient and is known to be significant in fullerene/polymer and fullerene/nanocrystal blends.[41]

Upon photoexcitation in the infrared regime only the PbS NCs contribute to the photocurrent via electron transfer to C_{60}. In the majority of devices the photocurrent observed in the infrared was found to be weaker above ≈700 nm further suggesting that the charge transfer process from PbS NC to C_{60} is compromised by the presence of the NC ligands. To resolve this issue, a ligand exchange process was undertaken to replace the oleic acid ligands with a short-chain carboxylic acid as recently reported.[51] To compare the charge transfer process from the PbS NCs to C_{60} fullerites before and after the ligand exchange photoluminescence (PL) quenching measurements were undertaken on samples prepared in an identical manner to that used to fabricate devices and also on the devices themselves. The PL spectrum of a drop-cast PbS NC film and a PbS NC/fullerite composite before and following ligand exchange are shown in Figure 2a. Significant, though incomplete, quenching of the PbS NC PL is observed in the untreated PbS NC/fullerite films accompanied by a small blue shift (≈10 nm) of the emission peak which may occur due to a change in local dielectric constant. Following ligand exchange it can be seen that the PbS NC PL is almost completely quenched providing strong evidence of efficient electron transfer from PbS NC to C_{60} fullerite taking place. To further confirm that PL quenching is due to electron transfer, and not absorption by C_{60}, similar measurements were undertaken using a 808 nm excitation source yielding the same result (Supporting Information Figure S2b). Identical results were obtained from studies performed on both devices and glass substrates.

The photocurrent spectrum of a typical PbS NC/C_{60} fullerite device following ligand exchange is shown in Figure 2b for a variety of applied bias voltages and typically displays an order of magnitude increase in current over an untreated device (Supporting Information Figure S3). Unlike for the untreated device the photocurrent spectra in the visible region do not display any peaks characteristic of C_{60} absorption (Figure 1b). This, in combination with the overall increase in photocurrent, is a direct result of the improvement in charge transfer efficiency gained following ligand exchange which now enables the PbS NCs to contribute to the photocurrent across the full spectral range.

Following ligand exchange the formation of small regions of continuous PbS NCs films on the device are observed which may become conducting and give rise to a photocurrent without requiring charge transfer to C_{60}. Such a contribution prior to ligand exchange was ruled out as no photocurrent could be measured from PbS NC only devices at the applied biases used in the experiment. In order to further investigate the origin of the photocurrent following ligand exchange, photocurrent measurements of PbS NCs films were obtained and compared to the PbS NC/C_{60} fullerite devices also following ligand exchange (**Figure 3**). It can be seen that the photoresponse obtained from the treated PbS NC only device is lower as compared to PbS NC/C_{60} fullerite device. The photocurrent in the visible regime is highly enhanced where C_{60} fullerites are present. We can therefore conclude that the enhancement in the photocurrent following ligand exchange is not solely due to the PbS NCs. The contribution by the C_{60} fullerites can be

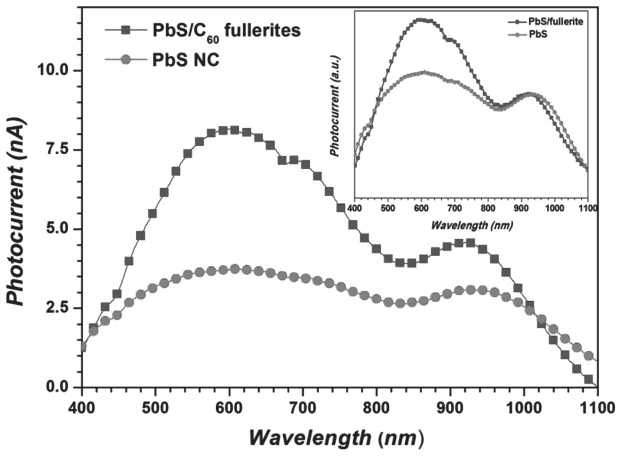

Figure 3. Photocurrent spectra obtained from a PbS NC only (circles) and PbS NC/C_{60} fullerite (squares) device. The inset shows the photocurrent normalized to the PbS NC maximum at ≈930 nm.

observed in the normalized spectra of PbS NC/C_{60} fullerite and PbS NC devices (inset Figure 3).

A further possibility remains however as to whether the photocurrent is due to charge transfer process or from the individual contribution of the PbS NCs and C_{60} fullerites. We assume that both of these processes may well contribute to the photocurrent though the relative energy level alignment between the PbS NCs and C_{60} and the significant PbS NC PL quenching following ligand exchange are strong signatures of charge transfer process. It is quite interesting that before the ligand exchange process PbS NCs were responsible for enhancing the C_{60} photoconductivity and extended their response to near IR wavelengths while after the ligand exchange process C_{60} fullerite were responsible for photocurrent enhancement in the visible range in PbS NC/C_{60} fullerite devices as compared to PbS NC only devices.

To characterize the device performance following ligand exchange in relation to other photodetectors several key figures of merits are provided. The responsivity R, is defined as ratio of photocurrent to the incident optical power:

$$R = \frac{J_{\text{ph}}}{L_{\text{Light}}} \tag{1}$$

where J_{ph} is the photocurrent and L_{Light} is the incident light intensity. **Figure 4**a shows the responsivity of the device as a function of applied bias and wavelength yielding values for example of ≈0.7 mA/W at 400 nm for a 20 V applied bias. A lower responsivity than might be expected may be due to decreased electron mobility of the C_{60} fullerites in air as it is well known that conductivity C_{60} crystals decreases drastically when exposed to oxygen.[52] The applied bias voltage and wavelength dependence of the responsivity is shown in Supporting Information Figure S4a. Under monochromatic illumination between 600 nm and 1000 nm a linear dependence on applied voltage is observed in the range measured whilst outside this region sub-linear behavior emerges. Having obtained R the external quantum efficiency (EQE) can be calculated using the formula:

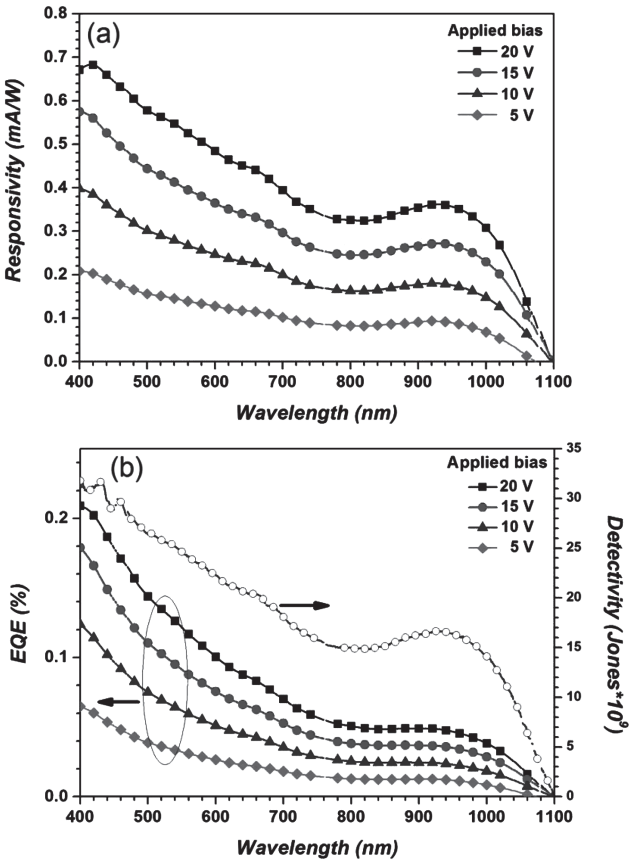

Figure 4. a) Spectral responsivity of a typical PbS NC/C_{60} fullerite device at varying applied voltage bias. b) EQE (closed symbols) at varying applied voltage bias and calculated detectivity (open circles) at an applied voltage bias of 15 V (light modulation frequency = 235 Hz) using the measured noise current.

$$EQE = R(hc)/(q\lambda) \tag{2}$$

where R is the responsivity, h is Plank's constant, c is the speed of light, q is the electron charge and λ is the wavelength. The figure of merit noise equivalent power (NEP) is the minimum optical power a photodetector can detect and is given by:

$$NEP = \sqrt{A\Delta f} \Big/ D^* \tag{3}$$

where A is the active area of the detector in cm^2, Δf is the electrical bandwidth in Hz and D^* is the detectivity given by

$$D^* = R\sqrt{A\Delta f} \Big/ I_{\text{n}} \tag{4}$$

where R is the responsivity in A/W and I_{n} is the noise current in amperes. The dark I–V characteristics are provided in Supporting Information Figure S4b and the transmission of a PbS NC/C_{60} fullerite film in Supporting Information Figure S5a. The detectivity, D^*, is an important figure of merit that allows the evaluation of the sensitivity of the device independent of device geometry and is usually reported in cm $Hz^{1/2}$ W^{-1} or Jones. Figure 4b shows the EQE and detectivity as a function of wavelength. The internal quantum efficiency (IQE) is found

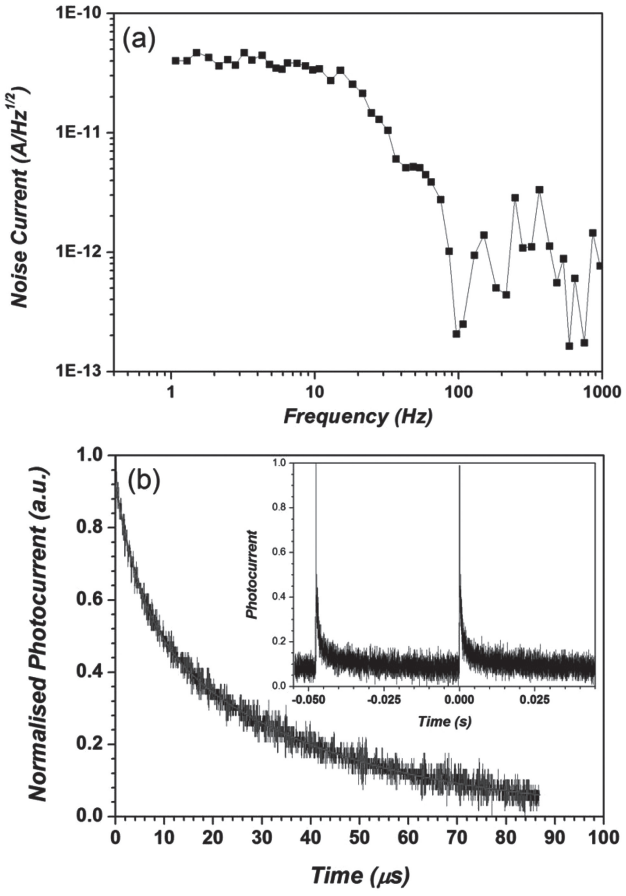

Figure 5. a) Dark current noise density of a typical PbS NC/C_{60} fullerite device as a function of frequency. b) Transient photocurrent response measured at 500 nm using an ≈8 ns laser pulse (repetition rate = 21 Hz) with an applied device bias voltage of 10 V. The inset to (b) shows two excitation cycles.

to be 1.5 to 2 times that of the EQE (Supporting Information Figure S5b). The device shows a detectivity in the range ≈10^{10} Jones with a peak detectivity ≈3.2 × 10^{10} Jones at 400 nm. These detectivity values are higher than previously reported values obtained from PbS NC/PCBM devices and are close to commercial near-IR detectors. Given that that our devices are fabricated and operated in air these values are of great significance.

Additionally, the sensitivity of the PbS NC/C_{60} fullerite photodetector device can be increased to longer wavelengths (e.g., 1350 nm) via tuning of the NC diameter (Supporting Information Figure S6). Measurement of the photodetector noise current shows a typical reduction with increasing frequency up to ≈100 Hz above which it becomes frequency independent and fluctuates at ≈1pA/$\sqrt{Hz}$, **Figure 5**a. In order to quantify the transient response of the devices the photocurrent was measured under 500 nm pulsed laser irradiation (≈8 ns pulse width at 21 Hz, ≈4.67 μJ) with the device bias voltage set to 10 V. The devices show a short (<40 ns) rise time followed by bi-exponential photocurrent decay with characteristic lifetimes of τ_1 = 5.3 μs ± 0.1 μs and τ_2 = 37.8 μs ± 0.7 μs (Figure 5b). The shorter of these times is similar to the measured radiative lifetime of the PbS NCs and thus may be related to the decay of excited states within the NCs.[53] The longer lifetime requires further study to fully understand its origin but may be related to the removal of trapped charges within the PbS NC/C_{60} fullerite composite. Further detailed dynamical studies will be reported in due course. In contrast to conventional detector technologies based on Si and InGaAs which require high temperature processing and are high cost, our findings are relevant for possible applications of PbS NC/C_{60} fullerite composite for the fabrication of a low cost, solution processed multispectral photodetector.

It is of interest to compare the performance of the above reported devices with those reported for devices based on PbS NC/PCBM blends.[38] However, given the difference in both device structure and measurement conditions (high-vacuum vs. ambient air in our studies) the only comparable parameter is D^*. Szendrei et al.[38] report a value of $D^* = 2.5 \times 10^{10}$ Jones provided at a single wavelength (1200 nm), determined using the noise current. In our studies values of D^* are of the order 10^{10} Jones for the PbS NC/C_{60} fullerite devices across a wide spectral range (again determined using the actual measured noise current) and are thus comparable. To enable a more appropriate means of comparing the use of C_{60} fullerites with PCBM as an alternative material we have fabricated (using the same experimental procedure) PbS NC/PCBM devices and characterized their performance operating under ambient air conditions. The absorption of the PbS NC/PCBM blend displays characteristic absorption from the PbS NCs and PCBM (Supporting Information Figure S7a). In these devices no crystal formation similar to the C_{60} fullerites is observed due to the non-symmetric nature of PCBM. None of the PbS NC/PCBM blend devices studied displayed any photocurrent prior to PbS NC ligand exchange (Supporting Information Figure S7b) unlike in the devices we report, where C_{60} is active as discussed above, suggesting that PCBM is not active in these devices.

Following ligand exchange the PbS NC/PCBM device becomes active displaying a photoresponse with a responsivity of ≈0.8 mA/W at 400 nm and ≈0.3 at 900 nm (Supporting Information Figure S8). Comparison of the photoresponse with the PbS NC:PCBM absorption shows that absorption of light by PCBM does not contribute to the response (evidenced by the lack of corresponding peak at ≈500 nm). These PbS NC/PCBM devices display a detectivity of ≈10^8 Jones across the near-IR region covering ≈700 nm to ≈1000 nm and ≈10^9 Jones in the visible region (Supporting Information Figure S9).

The above reported work therefore demonstrates that PbS NC/C_{60} fullerite devices do show an improved performance over PbS NC/PCBM devices fabricated and characterized under identical conditions. Furthermore, we also demonstrate that PbS NC/C_{60} fullerite devices fabricated and measured under ambient air conditions are able to match the performance of PbS NC/PCBM devices fabricated and operated under high vacuum conditions. Considering that C_{60} is a more favorable material with respect to its ability to accept electrons from large diameter PbS NCs (and so extending the spectral range further into the near-IR) these results are highly significant.

3. Conclusions

In summary, we have demonstrated a fast and convenient method for the fabrication of low-cost near-IR large area planar photodetector using PbS NCs and C_{60} fullerites. Through removing the need for a top electrode we also remove the requirement for a transparent conducting electrode and multiple deposition steps. The performance of the device is enhanced by replacing long oleic acid ligands with shorter ligands that resulted in improved charge transfer from PbS NCs to C_{60} fullerites. C_{60} fullerites not only act as an electron acceptor but also contribute to the photocurrent in the visible range. The photocurrent from the PbS NC/C_{60} fullerite device in the visible was found to be enhanced in the composite devices as compared to PbS NC or C_{60} fullerite only devices. The photodetector exhibits detectivity (D^*) $\approx 10^{10}$ from the near UV to the near-IR regime of the electromagnetic spectrum and the spectral coverage may be extended further into the near-IR via tuning of the PbS NC diameter. A fast (<40 ns) photocurrent rise time response is obtained upon excitation followed by a bi-exponential decay that is up to three orders of magnitude slower. These significant results open exciting opportunities for the fabrication of PbS NC/single C_{60} fullerite photodetectors for applications including optical communication, spectroscopy and biological sensing.

4. Experimental Section

Device Fabrication: 10 µm wide Interdigitated electrodes with an inter-electrode spacing of 10 µm (total device area = 5 mm × 5 mm) were formed on a SiO_2 (250 nm) on Si substrate. Prior to use the substrates were cleaned using acetone and isopropyl alcohol respectively for 5 minutes using ultrasonication prior to undergoing oxygen plasma treatment (100 W for 20 min). Primer and photoresist (Rohm and Hass MICROPOSIT S1813) were subsequently spin coated onto the substrates (3500 rpm for 35 s) followed by baking on a hot plate (115 °C for 1 min). The photoresist coated substrates were exposed to ultraviolet light through a pre-patterned mask at an energy dose of ≈40 mJ cm^{-2}. The pattern was developed (Rohm and Hass MF319 developer) by immersing the substrate for 4 min following which the substrates were washed using de-ionized water, dried with nitrogen, and placed within a sputterer for electrode deposition. An adhesion layer of chrome (≈10 nm) was sputtered first before deposition of ≈90 nm of gold followed by lift-off process in acetone to produce the desired pattern. Finally, substrates were again oxygen plasma treated to remove any residual photoresist prior to use.

C_{60} Fullerite Preparation: C_{60} fullerites were prepared using the liquid-liquid interfacial precipitation (LLIP) method. A stock solution (0.75 mg mL^{-1}) was prepared by dissolving pristine C_{60} powder (purity 99.9%, RMER corporation) in m-xylene (anhydrous > 99.9%, Sigma Aldrich). 2 mL of the stock solution was then added slowly to 2 mL of Isopropyl alcohol (IPA). After mixing, the solution was covered with parafilm and left for 2 h.

For sensitizing C_{60} fullerites with PbS NCs the above process was followed with the addition of few drops of PbS NCs (≈0.25 mL of ≈20 mg mL^{-1} in toluene) following the formation of a brownish-yellow suspension and the mixture immediately drop cast onto the interdigitated electrodes. The ratio of C_{60}:PbS NCs was ≈1:3.65 (wt%).

To fabricate PbS/PCBM devices identical methods were used to that described above (PCMB obtained from Solenne, 99% purity).

Ligand Exchange: To perform the ligand exchange process the device was treated in a mixture of 10% acetic acid in acetonitrile for 5 min.[51]

Electrical and Optical Measurements: Photocurrent was extracted by measuring the voltage drop across a load resistor connected in series with the device using lock in amplification (Signal Recovery 7265). A bias voltage to the device was provided by an adjustable Thurlby 30V 2A source. Illumination to the device was provided by 100 W tungsten lamp (Bentham IL1) passed through a monochromator (Bentham TMc300, 1200 g/mm grating blazed at 500 nm) and chopped at 235 Hz. Optical filters were placed in the path of the light to prevent second order grating reflections illuminating the device. The optical power falling on the device was measured separately using a calibrated Newport 818-UV detector. Responsivity was calculated by dividing the measured photocurrent by the optical power falling on the device. Noise current was measured using lock in amplifier (Signal Recovery 7265) in the frequency range 11 Hz to 1 kHz. The devices were biased using Thurlby 30V 2A source and the measurements were conducted in a optically and electrically shielded dark box. The reference frequency was provided by a signal generator with the lock-in amplifier acting as a narrow bandwidth amplifier directly outputting the noise current in the units given.

The transient response of the devices was measured by illuminating the device at 500 nm using a ≈8 ns pulse (≈4.76 µJ) from a Spectra-Physics VersaScan OPO operating at 21 Hz. The device was biased at 10 V and transient photocurrent signal recorded using a Tektronix TDS 3032B digital oscilloscope. All the measurements were done in air at room temperature.

Photoluminescence spectra were obtained under 514 nm excitation using Coherent Innova 300C Ar-ion laser (25 mW). The photoluminescence signal was obtained using the same monochromator and lock-in amplifier described above with a Newport 818-IG detector. A Varian Cary 5000 UV-Vis-NIR spectrophotometer was used to obtain absorption spectra.

Supporting Information

Supporting Information is available from the Wiley Online Library or from the author.

Acknowledgements

M.N.N. thanks MARA (University of Kuala Lumpur) for providing a PhD scholarship.

Received: September 27, 2012
Revised: November 29, 2012
Published online: March 11, 2013

[1] T. Rauch, M. Boberl, S. F. Tedde, J. Furst, M. V. Kovalenko, G. Hesser, U. Lemmer, W. Heiss, O. Hayden, *Nat. Photonics* **2009**, *3*, 332.
[2] G. Konstantatos, E. H. Sargent, *Nat. Nanotechnol.* **2010**, *5*, 391.
[3] S. Hoogland, V. Sukhovatkin, H. Shukla, J. Clifford, L. Levina, E. H. Sargent, *Opt. Express* **2008**, *16*, 6683.
[4] S. Kim, Y. T. Lim, E. G. Soltesz, A. M. De Grand, J. Lee, A. Nakayama, J. A. Parker, T. Mihaljevic, R. G. Laurence, D. M. Dor, L. H. Cohn, M. G. Bawendi, J. V. Frangioni, *Nat. Biotechnol.* **2004**, *22*, 93.
[5] X. Gao, Y. Cui, R. M. Levenson, L. W. K. Chung, S. Nie, *Nat. Biotechnol.* **2004**, *22*, 969.
[6] M. Ettenberg, *Adv. Imaging* **2005**, *20*, 29.
[7] X. Gong, M. Tong, Y. Xia, W. Cai, J. S. Moon, Y. Cao, G. Yu, C. L. Shieh, B. Nilsson, A. J. Heeger, *Science* **2009**, *325*, 1665.
[8] M. S. Arnold, J. D. Zimmerman, C. K. Renshaw, X. Xu, R. R. Lunt, C. M. Austin, S. R. Forrest, *Nano Lett.* **2009**, *9*, 3354.

[9] Y. Yao, Y. Liang, V. Shrotriya, S. Xiao, L. Yu, Y. Yang, *Adv. Mater* **2007**, *19*, 3979.
[10] I. W. Hwang, C. Soci, D. Moses, Z. Zhu, D. Waller, R. Gaudiana, C. J. Brabec, A. J. Heeger, *Adv. Mater.* **2007**, *19*, 2307.
[11] F. W. Wise, *Acc. Chem. Res.* **2000**, *33*, 773.
[12] J. P. Clifford, G. Konstantatos, K. W. Johnston, S. Hoogland, L. Levina, E. H. Sargent, *Nat. Nanotechnol.* **2009**, *4*, 40.
[13] G. Konstantatos, J. Clifford, L. Levina, E. H. Sargent, *Nat. Photonics* **2007**, *1*, 531.
[14] G. Konstantatos, I. Howard, A. Fischer, S. Hoogland, J. Clifford, E. Klem, L. Levina, *Nature* **2006**, *442*, 180.
[15] G. Konstantatos, M. Badioli, L. Gaudreau, J. Osmond, M. Bernechea, F. P. G. de Arquer, F. Gatti, F. H. L. Koppens, *Nat. Nanotechnol.* **2012**, *7*, 363.
[16] L. Vj, J. Oh, A. P. Nayak, A. M. Katzenmeyer, K. H. Gilchrist, S. Grego, N. P. Kobayashi, S. Y. Wang, A. A. Talin, N. K. Dhar, M. S. Islam, *IEEE J. Sel. Quantum Electron.* **2011**, *17*, 1002.
[17] C. Soci, A. Zhang, X.-Y. Bao, H. Kim, Y. Lo, D. Wang, *J. Nanosci. Nanotechnol.* **2010**, *10*, 1430.
[18] X. Zhang, J. Jie, W. Zhang, C. Zhang, L. Luo, Z. He, X. Zhang, W. Zhang, C. Lee, S. Lee, *Adv. Mater.* **2008**, *20*, 2427.
[19] G. A. O'Brien, A. J. Quinn, D. A. Tanner, G. Redmond, *Adv. Mater.* **2006**, *18*, 2379.
[20] R. C. Haddon, A. S. Perel, R. C. Morris, T. T. M. Palstra, A. F. Hebard, R. M. Fleming, *Appl. Phys. Lett.* **1995**, *67*, 121.
[21] C. M. Varma, J. Zaanen, K. Raghavachari, *Science* **1991**, *254*, 989.
[22] K. Ogawa, T. Kato, A. Ikegami, H. Tsuji, N. Aoki, Y. Ochiai, J. P. Bird, *Appl. Phys. Lett.* **2006**, *88*, 112109.
[23] S. L. Michael P. Larsson, *Rom. J. Interface Sci. Technol.* **2005**, *8*, 305.
[24] Y. J. Xing, G. Y. Jing, J. Xu, D. P. Yu, H. B. Liu, Y. L. Li, *Appl. Phys. Lett.* **2005**, *87*, 263117.
[25] T. D. Anthopoulos, B. Singh, N. Marjanovic, N. S. Sariciftci, A. M. Ramil, H. Sitter, M. Colle, D. M. d. Leeuw, *Appl. Phys. Lett.* **2006**, *89*, 213504.
[26] L. C. Chong, V. Stolojan, G. Wagner, S. R. P. Silva, R. J. Curry, *J. Mater. Chem.* **2008**, *18*, 4808.
[27] D. M. N. M. Dissanayake, R. A. Hatton, T. Lutz, C. E. Giusca, R. J. Curry, S. R. P. Silva, *Appl. Phys. Lett.* **2007**, *91*, 133506.
[28] D. M. N. M. Dissanayake, R. A. Hatton, T. Lutz, R. J. Curry, S. R. P. Silva, *Nanotechnology* **2009**, *20*, 245202.
[29] K. Miyazawa, Y. Kuwasaki, K. Hamamoto, S. Nagata, A. Obayashi, M. Kuwabara, *Surf. Interface Anal.* **2003**, *35*, 117.
[30] L. Wang, B. Liu, D. Liu, M. Yao, Y. Hou, S. Yu, T. Cui, D. Li, G. Zou, A. Iwasiewicz, B. Sundqvist, *Adv. Mater.* **2006**, *18*, 1883.
[31] L. C. Chong, J. Sloan, G. Wagner, S. R. P. Silva, R. J. Curry, *J. Mater. Chem.* **2008**, *18*, 4808.
[32] M. Sathish, K. Miyazawa, J. P. Hill, K. Ariga, *J. Am. Chem. Soc.* **2009**, *131*, 6372.
[33] Y. Jin, R. J. Curry, J. Sloan, R. A. Hatton, L. C. Chong, N. Blanchard, V. Stolojan, H. W. Kroto, S. R. P. Silva, *J. Mater. Chem.* **2006**, *16*, 3715.
[34] M. Tachibana, K. Kobayashi, T. Uchida, K. Kojima, M. Tanimura, K. Miyazawa, *Chem. Phys. Lett.* **2003**, *374*, 279.
[35] H. Li, B. C. K. Tee, J. J. Cha, Y. Cui, J. W. Chung, S. Y. Lee, Z. Bao, *J. Am. Chem. Soc.* **2012**, *134*, 2760.
[36] G. Lu, L. Li, X. Yang, *Small* **2008**, *4*, 601.
[37] A. Biebersdorf, R. Dietmüller, A. S. Susha, A. L. Rogach, S. K. Poznyak, D. V. Talapin, H. Weller, T. A. Klar, J. Feldmann, *Nano Lett.* **2006**, *6*, 1559.
[38] K. Szendrei, F. Cordella, M. V. Kovalenko, M. Böberl, G. Hesser, M. Yarema, D. Jarzab, O. V. Mikhnenko, A. Gocalinska, M. Saba, F. Quochi, A. Mura, G. Bongiovanni, P. W. M. Blom, W. Heiss, M. A. Loi, *Adv. Mater.* **2009**, *21*, 683.
[39] T. P. Osedach, N. Zhao, S. M. Geyer, L.-Y. Chang, D. D. Wanger, A. C. Arango, M. C. Bawendi, V. Bulović, *Adv. Mater.* **2010**, *22*, 5250.
[40] S. Pichler, T. Rauch, R. Seyrkammer, M. Boberl, S. F. Tedde, J. Furst, M. V. Kovalenko, U. Lemmer, O. Hayden, W. Heiss, *Appl. Phys. Lett.* **2011**, *98*, 053304.
[41] G. Itskos, A. Othonos, T. Rauch, S. F. Tedde, O. Hayden, M. V. Kovalenko, W. Heiss, S. A. Choulis, *Adv. Energy Mater.* **2011**, *1*, 802.
[42] D. Jarzab, K. Szendrei, M. Yarema, S. Pichler, W. Heiss, M. A. Loi, *Adv. Funct. Mater.* **2011**, *21*, 1988.
[43] D. C. Coffey, A. J. Ferguson, N. Kopidakis, G. Rumbles, *ACS Nano* **2010**, *4*, 5437.
[44] C. W. Chu, Y. Shao, V. Shrotriya, Y. Yang, *Appl. Phys. Lett.* **2005**, *86*, 243506.
[45] R. J. Davis, M. T. Lloyd, S. R. Ferreira, M. J. Bruzek, S. E. Watkins, L. Lindell, P. Sehati, M. Fahlman, J. E. Anthony, J. W. P. Hsu, *J. Mater. Chem.* **2011**, *21*, 1721.
[46] C. W. Chu, V. Shrotriya, G. Li, Y. Yang, *Appl. Phys. Lett.* **2006**, *88*, 153504.
[47] A. Gocalińska, M. Saba, F. Quochi, M. Marceddu, K. Szendrei, J. Gao, M. A. Loi, M. Yarema, R. Seyrkammer, W. Heiss, A. Mura, G. Bongiovanni, *J. Phys. Chem. Lett.* **2010**, *1*, 1149.
[48] D. M. N. M. Dissanayake, T. Lutz, R. J. Curry, S. R. P. Silva, *Appl. Phys. Lett.* **2008**, *93*, 043501.
[49] B. R. Hyun, Y.-W. Zhong, A. C. Bartnik, L. Sun, H. D. Abruña, F. W. Wise, J. D. Goodreau, J. R. Matthews, T. M. Leslie, N. F. Borrelli, *ACS Nano* **2008**, *2*, 2206.
[50] T. Agostinelli, M. Caironi, D. Natali, M. Sampietro, P. Biagioni, M. Finazzi, L. Duo, *J. Appl. Phys.* **2007**, *101*, 114504.
[51] M. H. Zarghami, Y. Liu, M. Gibbs, E. Gebremichael, C. Webster, M. Law, *ACS Nano* **2010**, *4*, 2475.
[52] T. Arai, Y. Murakami, H. Suematsu, K. Kikuchi, Y. Achiba, I. Ikemoto, *Solid State Commun.* **1992**, *84*, 827.
[53] M. N. Nordin, K. N. Bourdakos, R. J. Curry, *Phys. Chem. Chem. Phys.* **2010**, *12*, 7371.